The effect of nonlinearities on the frequency response of a round jet

Ubaid Ali Qadri and Peter J. Schmid

Department of Mathematics, Imperial College London,

London, SW7 2AZ, United Kingdom

(Dated: April 5, 2017)

Abstract

We investigate the effect of nonlinearities on the frequency response of a round, incompressible jet. Experiments show that axisymmetric structures dominate the response of forced and unforced jets. In contrast, linear stability and frequency response analyses predict the asymmetric mode ($m = 1$) to be locally more unstable and globally more amplified than the axisymmetric mode ($m = 0$). We perform a weakly nonlinear expansion of the response of the flow to harmonic forcing and derive an asymptotic expression for the sum of this divergent series beyond its limit of validity. This expression compares reasonably well with the nonlinear gain up to forcing amplitudes an order of magnitude greater than the limit of validity of the weakly nonlinear expansion. For equal forcing amplitudes, the asymmetric mode dominates over the axisymmetric mode. This suggests that the projection of environmental forcing onto the individual azimuthal modes plays an important role in the preferred dynamics of round jets.

I. INTRODUCTION

Large-scale unsteady flow structures play an important role in the dynamics of laminar and turbulent jets, as they are responsible for a large proportion of the momentum and energy transfer taking place. Early experiments [1] have shown that, as the Reynolds number is increased, the unsteadiness takes the form of a sinusoid, then a helix, and finally axisymmetric vortex rings at a dominant (non-dimensional) frequency of $St \sim 0.3$ based on the jet diameter and jet exit velocity. For turbulent jets, the preferred frequency has been found to vary between $0.25 < St < 0.6$ based on the experimental set-up. In this study, however, we focus on laminar jets.

Several studies employed linear stability analyses to understand the mechanisms that determine the selection of the preferred frequency. Local stability analyses [2, 3] found that axisymmetric and helical perturbations are spatially amplified downstream of the jet exit plane. The competition between these two modes depends on the local flow profile and jet shear-layer thickness. Thin shear layers and top-hat flow profiles favor the axisymmetric mode, while thick shear layers and fully developed flow profiles favor the helical mode.

From a fully non-parallel perspective, the uniform density jet is globally stable [4], and behaves as a hydrodynamic amplifier. The flow experiences oscillations only in the presence of external forcing or noise, and amplifies these disturbances selectively. The unsteadiness arises from a superposition of all linear global eigenmodes with negative growth rates and thus cannot be modelled by a finite subset of global modes [4]. Instead, the dynamics of the flow are more appropriately represented by its response to external forcing [5]. Within a linear framework, this response can be quantified by calculating the optimal frequency response and identifying the forcing structure that is linearly most amplified due to the non-normality of the linear operator [6, 7]. For an isothermal jet, the optimal frequency response for axisymmetric forcing shows a dominant peak at $St \sim 0.45$ [8], but non-axisymmetric forcing structures are linearly more strongly amplified. It has been suggested that the discrepancy between experimental observations and the optimal frequency response analysis could be explained by the effects of turbulence and nonlinear saturation.

As the forcing amplitude is increased, nonlinearity acts to saturate the response and thus reduces the amplification. In a recent study, this saturation effect was explored for flow over a backward-facing step [9]. For small forcing amplitudes, the nonlinear saturation

was captured exactly using a weakly nonlinear expansion about the steady base flow. For larger forcing amplitudes, the nonlinear saturation could be captured accurately using a self-consistent model in which the linear frequency response is coupled to the mean flow via the Reynolds stresses. The results demonstrated that the interaction between the first harmonic and the steady base flow is more important in determining the nonlinear saturation than the higher harmonics.

In this present study, we investigate the effects of nonlinearity on the frequency response of a laminar isothermal jet. Our aim is to understand how nonlinear saturation affects the amplification of different azimuthal modes, and to understand why experiments show a preference for axisymmetric structures, even though helical modes are linearly more amplified.

II. PROBLEM FORMULATION

A. Flow configuration

We study the motion of a round jet of incompressible fluid exiting from a circular pipe into a large cylindrical domain of length X_{max} and radius R_{max}. The fluid is described by its state vector, $\mathbf{q} = (\mathbf{u}, p)^T$, which contains the pressure p and the velocities $\mathbf{u} = (u_x, u_r, u_\theta)^T$ in the axial (x), radial (r), and azimuthal (θ) directions, respectively. The geometry is identical to the one used by Garnaud *et al.* [8] to study the optimal linear frequency response of the jet. The flow variables and domain lengths are made non-dimensional using the centerline axial velocity U_{in} at the inlet and the pipe diameter D.

The motion of the fluid is governed by the forced incompressible Navier–Stokes (NS) equations in non-dimensional form, given as

$$\begin{aligned} \nabla \cdot \mathbf{u} &= 0, \\ \frac{\partial \mathbf{u}}{\partial t} + \mathbf{u} \cdot \nabla \mathbf{u} + \nabla p - \frac{1}{Re} \nabla^2 \mathbf{u} &= \mathbf{f}, \end{aligned} \tag{1}$$

where the Reynolds number, Re, is defined in terms of U_{in} and D, and $\mathbf{f}$ represents a body forcing. We assume that the forcing is harmonic in nature and has a small-amplitude, $\mathbf{f}(\mathbf{x}, t) = \epsilon(\hat{\mathbf{f}}(\mathbf{x}) e^{\mathrm{i}\omega_f t} + \hat{\mathbf{f}}^*(\mathbf{x}) e^{-\mathrm{i}\omega_f t})$, where the superscript * denotes the complex conjugate.

B. Weakly nonlinear analysis

The response can then be represented by an asymptotic expansion around a steady base flow in terms of the small parameter ϵ. A consistent form of this expansion is given by a summation of steady and harmonic terms [9]

$$\mathbf{q}(\mathbf{x},t) = \bar{\mathbf{q}}_{0,0}(\mathbf{x}) + \sum_{n=1}^{\infty} \epsilon^n \bar{\mathbf{q}}_{0,n}(\mathbf{x}) + \sum_{p=1}^{\infty} e^{\mathrm{i}p\omega_f t} \sum_{n=1}^{\infty} \epsilon^n \hat{\mathbf{q}}_{p,n}(\mathbf{x}) + \text{c.c.}, \tag{2}$$

where the index p represents the frequency harmonic and n represents the order of the expansion. Assuming that the steady base flow is axisymmetric, we decompose the forcing and higher-order corrections into a sum of modes of azimuthal wavenumber m

$$\mathbf{f}(\mathbf{x},t) = \sum_{m=0}^{\infty} \epsilon \hat{\mathbf{f}}_m(x,r) e^{\mathrm{i}m\theta} e^{\mathrm{i}\omega_f t} + \text{c.c.} \tag{3}$$

$$\mathbf{q}(\mathbf{x},t) = \bar{\mathbf{q}}_{0,0}(x,r) + \sum_{n=1}^{\infty} \epsilon^n \sum_{m=-\infty}^{\infty} \bar{\mathbf{q}}_{m,0,n}(x,r) e^{\mathrm{i}m\theta} + \sum_{p=1}^{\infty} e^{\mathrm{i}p\omega_f t} \sum_{n=1}^{\infty} \epsilon^n \sum_{m=0}^{\infty} \hat{\mathbf{q}}_{m,p,n}(x,r) e^{\mathrm{i}m\theta} + \text{c.c.} \tag{4}$$

The rotational symmetry of the problem implies that $\bar{\mathbf{q}}_{-k,0,n} = \bar{\mathbf{q}}^*_{k,0,n}$ and that the complex conjugate terms (c.c.) are of the form $\hat{\mathbf{q}}^*_{m,p,n} e^{-\mathrm{i}(m\theta+\omega_f t)}$. We substitute this expression into (1) and equate terms at different orders of ϵ.

1. *At zeroth order, ϵ^0*

We obtain a set of equations for the axisymmetric solution of the steady base flow, which we label $\bar{\mathbf{q}}_0 = (\bar{\mathbf{u}}_0, \bar{p}_0)^T =$ for ease of reference. It satisfies

$$\begin{aligned} \nabla \cdot \bar{\mathbf{u}}_0 &= 0, \\ \bar{\mathbf{u}}_0 . \nabla \bar{\mathbf{u}}_0 + \nabla \bar{p}_0 - \frac{1}{Re} \nabla^2 \bar{\mathbf{u}}_0 &= 0. \end{aligned} \tag{5}$$

which can be written in the compact form $\mathcal{N}(\bar{\mathbf{u}}_0) = 0$.

2. *At first order, ϵ^1*

The first-order steady correction terms for all azimuthal modes are zero, $\bar{\mathbf{q}}_{m,0,1} = 0$; furthermore, the different azimuthal modes of the first harmonic are independent. This

yields an expression for the linear frequency response as a sum of responses for the individual azimuthal modes. We obtain

$$\sum_{m=0}^{\infty}(\mathrm{i}\omega_f\mathbf{B}-\mathbf{L}_m)\hat{\mathbf{q}}_{m,1,1}=\sum_{m=0}^{\infty}\hat{\mathbf{f}}_m e^{\mathrm{i}m\theta} \tag{6}$$

where the linear operators $\mathbf{B}$ and $\mathbf{L}_m$ are defined such that

$$\mathbf{B}=\begin{pmatrix} I & 0 \\ 0 & 0 \end{pmatrix}, \qquad \mathbf{L}_m=\begin{pmatrix} -\nabla_0\bar{\mathbf{u}}_0\cdot(.)-\bar{\mathbf{u}}_0\cdot\nabla_m(.)+\frac{1}{Re}\nabla_m^2(.) & -\nabla_m(.) \\ \nabla_m\cdot(.) & 0 \end{pmatrix}.$$

3. At second order, ϵ^2

The second-order steady correction terms are obtained by solving inhomogeneous linear systems for all azimuthal modes independently. These linear systems are forced by the Reynolds stress terms which represent the interactions between the first harmonic responses and their complex conjugates.

$$\mathbf{L}_m\bar{\mathbf{q}}_{m,0,2}e^{\mathrm{i}m\theta}=\begin{pmatrix} \sum_{j=m}^{\infty}(\hat{\mathbf{u}}^*_{j-m,1,1}.\nabla\hat{\mathbf{u}}_{j,1,1}+\hat{\mathbf{u}}_{j,1,1}.\nabla\hat{\mathbf{u}}^*_{j-m,1,1}) \\ 0 \end{pmatrix} e^{\mathrm{i}m\theta}. \tag{7}$$

The unsteady component of the second-order terms is given by the second-order frequency response for the second harmonic,

$$(2\mathrm{i}\omega_f\mathbf{B}-\mathbf{L}_m)\hat{\mathbf{q}}_{m,2,2}e^{\mathrm{i}m\theta}=\begin{pmatrix} -\sum_{j=0}^{m}(\hat{\mathbf{u}}_{j,1,1}.\nabla\hat{\mathbf{u}}_{m-j,1,1}) \\ 0 \end{pmatrix} e^{\mathrm{i}m\theta}. \tag{8}$$

4. At third order, ϵ^3

There is no third-order steady component. The unsteady component consists of the third-order correction to the frequency response for the first harmonic, according to

$$(\mathrm{i}\omega_f\mathbf{B}-\mathbf{L}_m)\hat{\mathbf{q}}_{m,1,3}e^{\mathrm{i}m\theta}=\begin{pmatrix}-\sum_{j=-\infty}^{m}(\bar{\mathbf{u}}_{j,0,2}.\nabla\hat{\mathbf{u}}_{m-j,1,1}+\hat{\mathbf{u}}_{m-j,1,1}.\nabla\bar{\mathbf{u}}_{j,0,2})\\ 0\end{pmatrix}e^{\mathrm{i}m\theta}$$
$$+\begin{pmatrix}-\sum_{j=m}^{\infty}(\hat{\mathbf{u}}^*_{j-m,1,1}.\nabla\hat{\mathbf{u}}_{j,2,2}+\hat{\mathbf{u}}_{j,2,2}.\nabla\hat{\mathbf{u}}^*_{j-m,1,1})\\ 0\end{pmatrix}e^{\mathrm{i}m\theta}, \tag{9}$$

and the third-order frequency response for the third harmonic,

$$(3\mathrm{i}\omega_f\mathbf{B}-\mathbf{L}_m)\hat{\mathbf{q}}_{m,3,3}e^{\mathrm{i}m\theta}=\begin{pmatrix}-\sum_{j=0}^{m}(\hat{\mathbf{u}}_{j,1,1}.\nabla\hat{\mathbf{u}}_{m-j,2,2}+\hat{\mathbf{u}}_{m-j,2,2}.\nabla\hat{\mathbf{u}}_{j,1,1})\\ 0\end{pmatrix}e^{\mathrm{i}m\theta}. \tag{10}$$

Higher-order terms can be calculated in a similar manner, if needed.

C. An expression for the gain

The frequency amplification or gain is measured by the ratio of the kinetic energy of the response to the kinetic energy of the forcing, integrated over the domain Ω of volume V shown in figure 1 and averaged over one period. This is equivalent to the ratio of the squared L^2 norms of the unsteady components of the response and the forcing. Using the expression in (2), we obtain

$$G=\frac{\frac{1}{T}\int_0^T\int_\Omega\mathbf{u}'^2dV}{\frac{1}{T}\int_0^T\int_\Omega\mathbf{f}^2dV}, \tag{11}$$
$$=\frac{\epsilon^2\int_\Omega(\hat{\mathbf{u}}^*_{1,1}\hat{\mathbf{u}}_{1,1}+2\epsilon^2\hat{\mathbf{u}}^*_{1,1}\hat{\mathbf{u}}_{1,3}+\epsilon^2\hat{\mathbf{u}}^*_{2,2}\hat{\mathbf{u}}_{2,2}+\mathcal{O}(\epsilon^4))dV}{\epsilon^2\int_\Omega\hat{\mathbf{f}}^*\hat{\mathbf{f}}dV},$$
$$=G_1+\epsilon^2(G_{1,13}+G_{2,2})+\mathcal{O}(\epsilon^4). \tag{12}$$

In general, the forcing consists of a superposition of many azimuthal modes, leading to each component of the flow response containing multiple azimuthal modes, $\hat{\mathbf{u}}_{p,n}=\sum_{m=0}^{N}\hat{\mathbf{u}}_{m,p,n}$. For example, non-axisymmetric steady corrections to the base flow, $\bar{\mathbf{q}}_{m\neq0,0,2}$ arise due to

interaction between the axisymmetric and non-axisymmetric modes of the first harmonic. For the simpler case of forcing consisting of only one azimuthal mode, we present here expressions for the flow response. These expressions can then be substituted into (12) to calculate the gain resulting from forcing with different azimuthal wavenumbers.

1. $m = 0$ *forcing*

In the presence of only axisymmetric forcing, all components of the response are merely axisymmetric. The basic form of the flow response is then given by

$$\mathbf{q} = \bar{\mathbf{q}}_0 + \epsilon^2 \bar{\mathbf{q}}_{0,0,2} + \epsilon(\hat{\mathbf{q}}_{0,1,1} + \epsilon^2 \hat{\mathbf{q}}_{0,1,3}) e^{\mathrm{i}\omega_f t} + \epsilon^2 \hat{\mathbf{q}}_{0,2,2} e^{2\mathrm{i}\omega_f t} + \epsilon^3 \hat{\mathbf{q}}_{0,3,3} e^{3\mathrm{i}\omega_f t} + \mathcal{O}(\epsilon^4). \tag{13}$$

2. $m = 1$ *forcing*

In the presence of forcing with only $m = 1$, i.e., $\mathbf{f} = \hat{\mathbf{f}}_1 e^{\mathrm{i}\theta + \mathrm{i}\omega_f t}$, the forcing produces an axisymmetric steady modification of the base flow, a first hamonic with $m = 1$, a second harmonic with $m = 2$, and a third harmonic with $m = 3$. The corresponding flow response is given by

$$\mathbf{q} = \bar{\mathbf{q}}_0 + \epsilon^2 \bar{\mathbf{q}}_{0,0,2} + \epsilon(\hat{\mathbf{q}}_{1,1,1} + \epsilon^2 \hat{\mathbf{q}}_{1,1,3}) e^{\mathrm{i}\theta + \mathrm{i}\omega_f t} + \epsilon^2 \hat{\mathbf{q}}_{2,2,2} e^{2\mathrm{i}\theta + 2\mathrm{i}\omega_f t} + \epsilon^3 \hat{\mathbf{q}}_{3,3,3} e^{3\mathrm{i}\theta + 3\mathrm{i}\omega_f t} + \mathcal{O}(\epsilon^4). \tag{14}$$

3. $m = 2$ *forcing*

In the presence of forcing with only $m = 2$, i.e., $\mathbf{f} = \hat{\mathbf{f}}_1 e^{2\mathrm{i}\theta + \mathrm{i}\omega_f t}$, the forcing produces an axisymmetric steady modification of the base flow, a first harmonic with $m = 2$, a second harmonic with $m = 4$, and a third harmonic with $m = 6$. The corresponding flow response is given by

$$\mathbf{q} = \bar{\mathbf{q}}_0 + \epsilon^2 \bar{\mathbf{q}}_{0,0,2} + \epsilon(\hat{\mathbf{q}}_{2,1,1} + \epsilon^2 \hat{\mathbf{q}}_{2,1,3}) e^{\mathrm{i}\theta + \mathrm{i}\omega_f t} + \epsilon^2 \hat{\mathbf{q}}_{4,2,2} e^{4\mathrm{i}\theta + 2\mathrm{i}\omega_f t} + \epsilon^3 \hat{\mathbf{q}}_{6,3,3} e^{6\mathrm{i}\theta + 3\mathrm{i}\omega_f t} + \mathcal{O}(\epsilon^4). \tag{15}$$

III. NUMERICAL IMPLEMENTATION

The governing equations are multiplied by the radial coordinate r, recast into a weak formulation, and discretized on the computational domain shown in figure 1 using the finite-

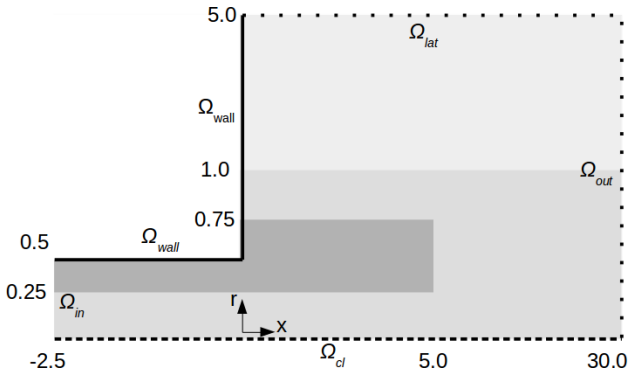

FIG. 1. Sketch of the computational domain used for the numerical solution by the finite element method, with $X_{max} = 30.0$ and $R_{max} = 5.0$. Darker shades of grey represent higher grid resolutions. The boundaries of the domain include the wall (Ω_{wall}), centerline (Ω_{cl}), outlet (Ω_{out}), lateral boundary (Ω_{lat}), and the inlet (Ω_{in}).

element method implemented in FreeFem++, based on modified versions of the scripts developed by Garnaud [4, 8] that are available online as the *femstab* package. We use Taylor-Hood elements for the velocity (P2) and pressure (P1) fields. The mesh consists of 157 444 triangles, and we have checked that doubling the resolution changes the weakly nonlinear gain coefficients by less than 1%.

No-slip Dirichlet conditions for the velocities are imposed along the wall, while viscous stress-free boundary conditions are applied at the outlet and along the lateral boundary. Along the centerline, homogeneous Dirichlet and Neumann conditions for the velocity components are used depending on the azimuthal mode being solved for. At the inlet to the pipe, we set the axial velocity to $u_x = \tanh(0.25(1 - 4r^2)D/(2\theta))$, where the parameter $D/(2\theta) = 12.5$ determines the thickness of the shear-layer. The steady base flow is obtained using the Newton-Raphson method. The sparse matrices and vectors associated with the solution of the linear systems in equations (6)-(10) are assembled in FreeFem++; matrix inversions are performed using the MUMPS package.

IV. RESULTS

We consider the response of a uniform density jet at $Re = 1000$ to a forcing with a Gaussian profile for the radial velocity at the jet exit plane given by $\hat{f}_r = \exp\left(-100(x^2 + (r - 0.5)^2)\right)$. First, we calculate the linear gain for this fixed forcing structure for azimuthal wavenumbers

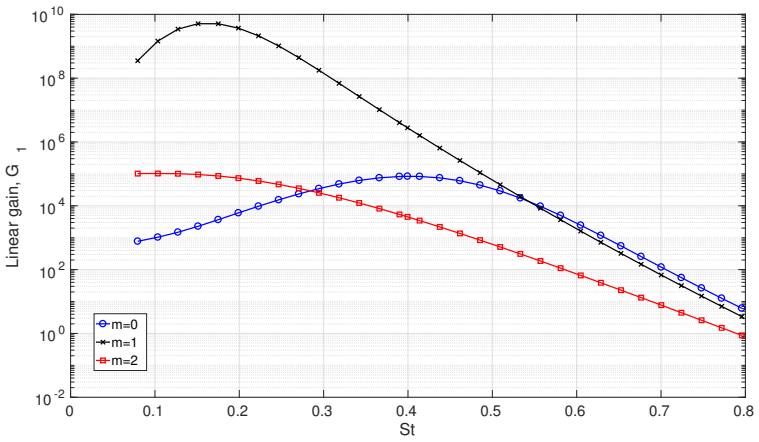

FIG. 2. The linear frequency response, G_1 for $m = 0$ (circles), $m = 1$ (crosses), and $m = 2$ (squares) at $Re = 1000$.

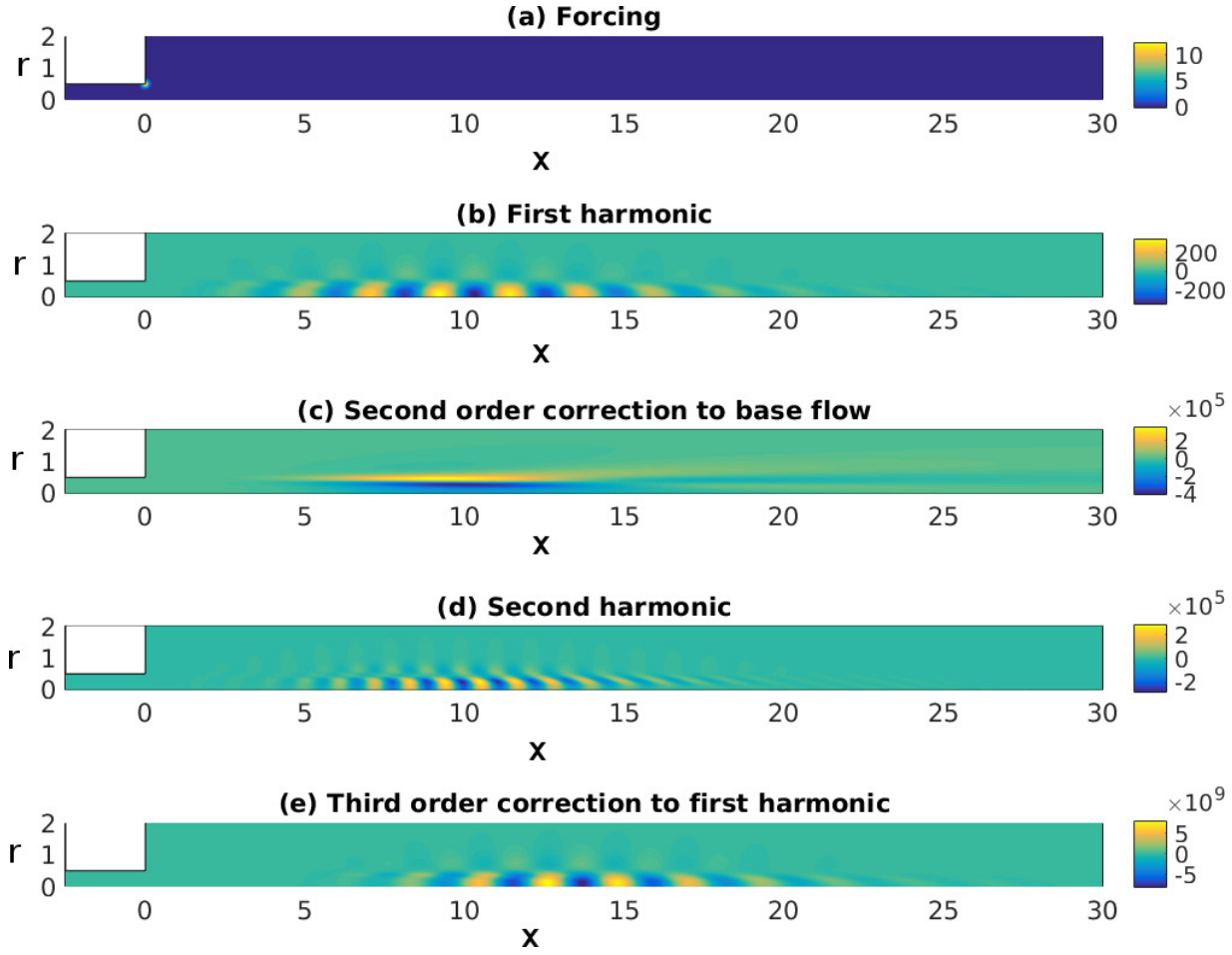

FIG. 3. The forcing (a) at $St = 0.40$ and the weakly nonlinear mode structures (b)-(e) for $m = 0$ at $Re = 1000$.

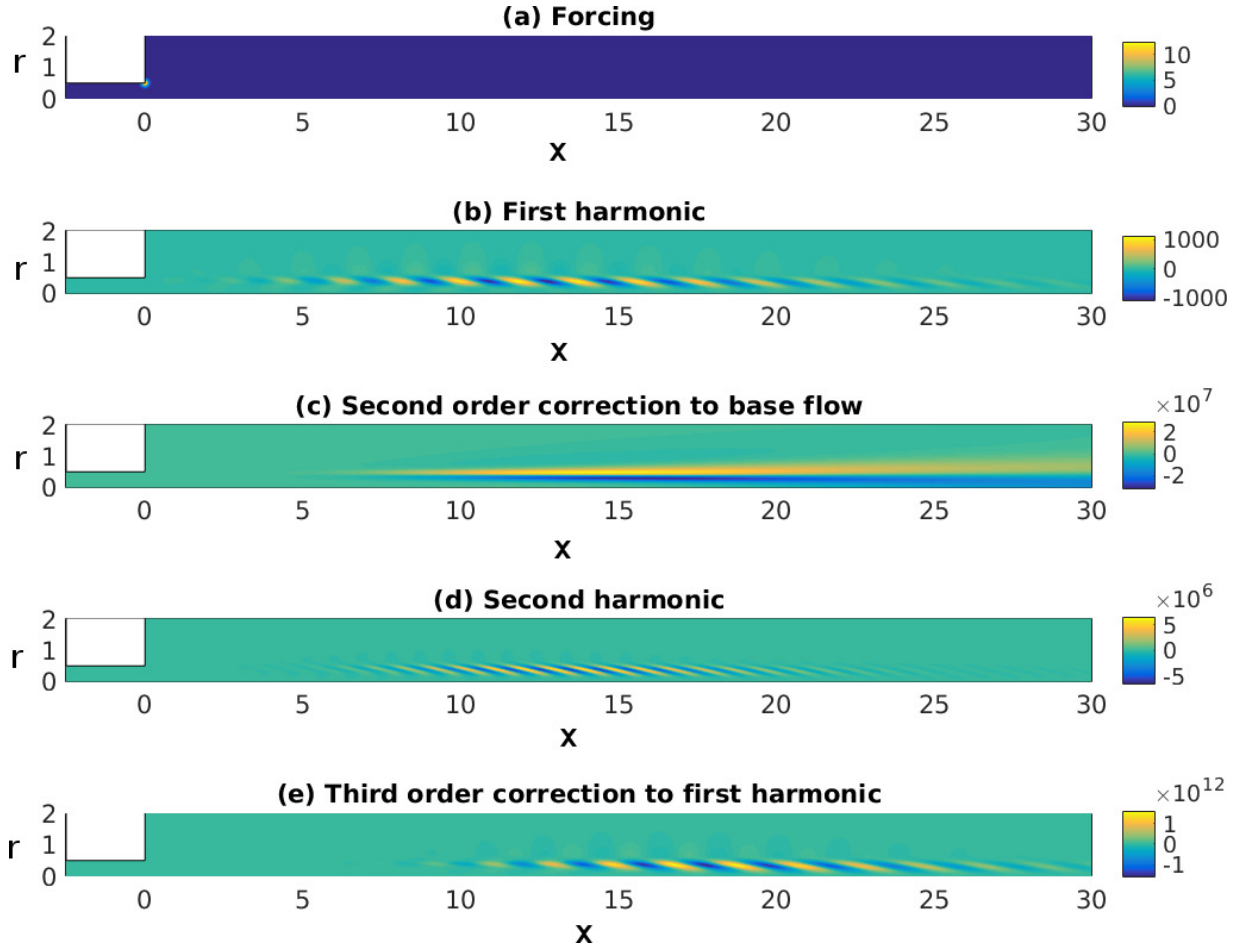

FIG. 4. The forcing (a) at $St = 0.40$ and the weakly nonlinear mode structures (b)-(e) for $m = 1$ at $Re = 1000$.

$m = 0, 1, 2$. The results are shown in figure 2 and are similar to those obtained for the optimal linear amplification in a model turbulent mean flow [8]. This confirms that this forcing structure is unbiased. There is a well-defined peak at $St \sim 0.4$ for a forcing with $m = 0$, but a forcing with an azimuthal wavenumber of $m = 1$ exhibits larger linear amplification.

We normalize the forcing such that $\int_\Omega \hat{\mathbf{f}}^* \hat{\mathbf{f}} dV = 1$ and then calculate the various harmonics and corrections as derived in section 2. The results are shown in figures 3 and 4 for forcings at $St = 0.40$ with $m = 0$ and $m = 1$. We notice that the responses for $m = 1$ have higher magnitudes and reach a maximum further downstream compared to $m = 0$. In addition, higher-order corrections also have larger magnitudes further downstream compared to the first harmonic.

We next investigate the effects of weak nonlinearity on the gain by calculating the higher-

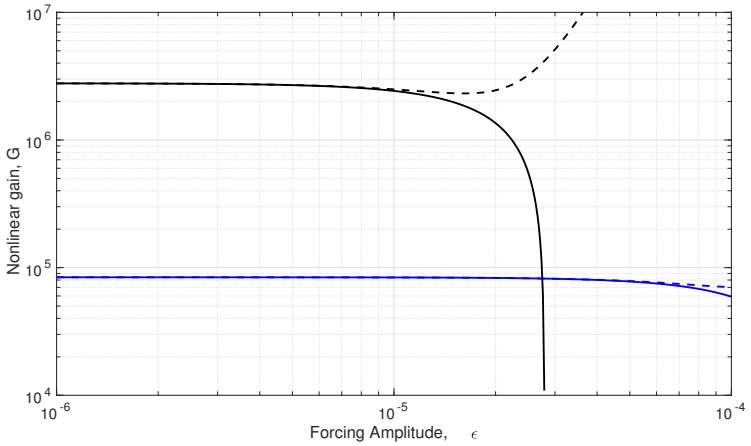

FIG. 5. The variation of the gain with forcing amplitude for forcing with $m = 0$ (blue) and $m = 1$ (black) for $St = 0.40$ at $Re = 1000$. The solid lines represent the second-order expression and the dashed lines represent the fourth-order expression for the gain.

order gain coefficients $G_{2,2}$ and $G_{1,13}$ as presented in (12). The second-order gain is shown in figure 5 for a forcing with $m = 0$ and $m = 1$ at $St = 0.40$. Even though $m = 1$ experiences greater linear amplification, as the forcing amplitude increases, the gain drops sharply and, above a forcing amplitude of $\epsilon = 3 \times 10^{-5}$, the $m = 0$ mode experiences greater amplification. The sharp drop motivates us to examine the effect of higher-order corrections by including fourth-order and fifth-order terms in the flow response. The gain is then given by the expression

$$G = G_1 + \epsilon^2(G_{1,13} + G_{2,2}) + \epsilon^4(G_{1,15} + G_{2,24} + G_{3,3} + G_{13,13}) + \mathcal{O}(\epsilon^6) \tag{16}$$

$$= G_1 + \epsilon^2 G_2 + \epsilon^2 G_4 + \mathcal{O}(\epsilon^6), \tag{17}$$

where the additional terms are defined as $G_{1,15} = 2\int_\Omega \hat{\mathbf{u}}^*_{1,1}\hat{\mathbf{u}}_{1,5}dV$, $G_{2,24} = 2\int_\Omega \hat{\mathbf{u}}^*_{2,2}\hat{\mathbf{u}}_{2,4}dV$, $G_{3,3} = \int_\Omega \hat{\mathbf{u}}^*_{3,3}\hat{\mathbf{u}}_{3,3}dV$, and $G_{13,13} = \int_\Omega \hat{\mathbf{u}}^*_{1,3}\hat{\mathbf{u}}_{1,3}dV$. The dashed lines in figure 5 represent the fourth-order expression for the gain. The fourth-order gain curves are divergent because the highest-order coefficient is positive. We examine this divergence in more detail by evaluating the weakly nonlinear coefficients for a range of Reynolds numbers $100 \leq Re \leq 1000$. We can group the coefficients at each order of the asymptotic expansion. In figure 6, we show how these coefficients vary with Reynolds number for $m = 0$ and $m = 1$. With the exception of low Reynolds numbers where the flow profile at the jet exit plane is signficantly different from the top-hat profile at the domain inlet, the gain coefficients show a near-perfect exponential

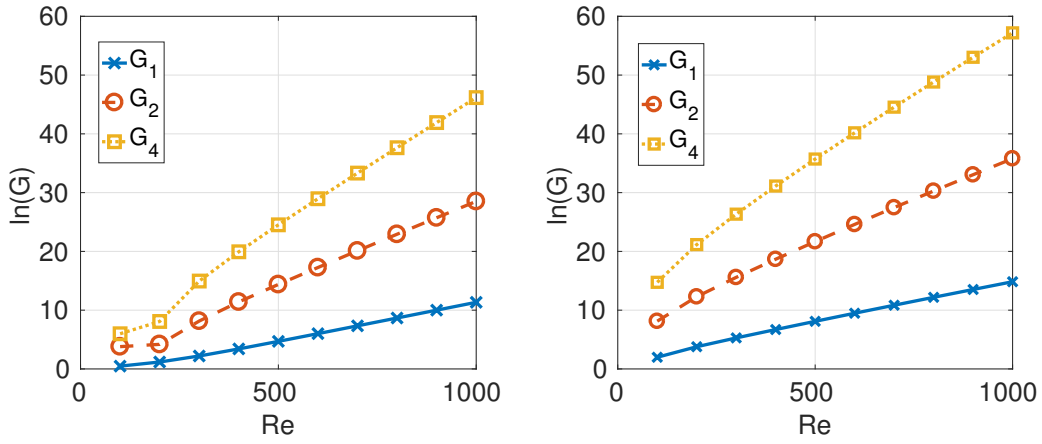

FIG. 6. The variation of the gain coefficients with Reynolds number for (a) $m = 0$, and (b) $m = 1$.

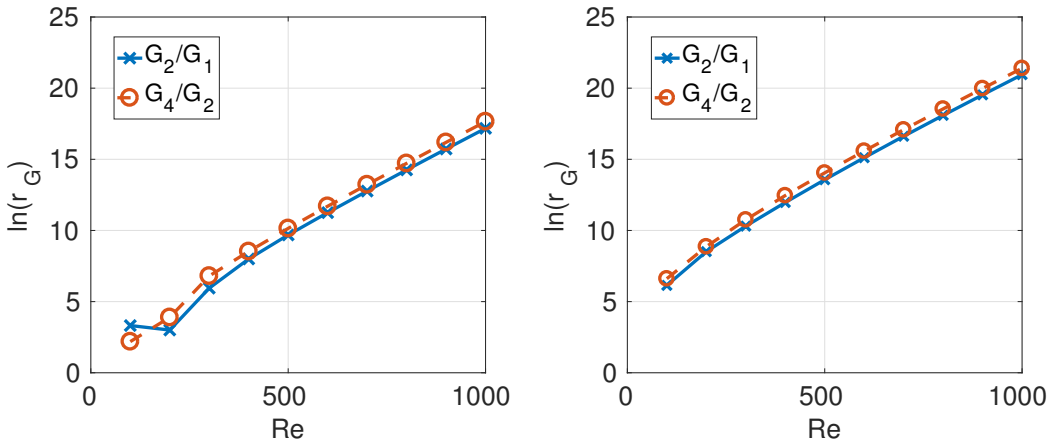

FIG. 7. The ratios of the first three gain coefficients with Reynolds number for (a) $m = 0$, and (b) $m = 1$.

dependence on the Reynolds number. This is directly related to the local properties of the flow. The condition number of the eigenvector matrix (and the resolvent norm) of the discrete Orr-Sommerfeld operator scales as $e^{\alpha Re^{\gamma}}$ for some α and $\gamma < 1$ [10]. For the flow considered here, we find that $G_1 \sim e^{0.013Re}$, $G_2 \sim e^{0.028Re}$ and $G_4 \sim e^{0.043Re}$ for both $m = 0$ and $m = 1$.

Plotting the ratios of the absolute values of the gain coefficients G_2/G_1, G_4/G_2 in figure 7, we notice that the ratios also vary roughly as $r_G \sim e^{0.013Re}$. From a physical perspective, this dependence is not entirely surprising. Looking at the weakly nonlinear gain coefficients in more detail (table I), the largest magnitude at each order is obtained for interactions

involving the first harmonic (and its corrections). At each order in the expansion, the corrections to the first harmonic are calculated using the first-order (linear) resolvent and a higher-order forcing term. The dominant contribution to this forcing term comes from the interaction between the steady correction to the base flow and the first harmonic (and its corrections) – the first term in (9). Similar behavior has also been observed for flow over a backward-facing step [9]. Therefore, it is not surprising that the scaling for the linear gain carries over in a multiplicative fashion to higher-order gain coefficients. To approximate the behavior of the gain as the forcing amplitude increases, we assume for now that the ratios between coefficients are equal and represent the weakly nonlinear asymptotic expansion as a geometric series of the form

$$\begin{aligned}\frac{G}{G_1} &= 1 - r_G\epsilon^2 + r_G^2\epsilon^4 - r_G^3\epsilon^6 \cdots \\ &= \sum_{n=0}^{\infty}(-r_G\epsilon^2)^n. \end{aligned} \tag{18}$$

where we set $r_G = G_2/G_1$. This can be represented as the power series

$$\frac{G}{G_1} \approx \frac{1}{1 + r_G\epsilon^2}, \tag{19}$$

with a radius of convergence $r_G\epsilon^2 = 1$. From this, we can deduce that the weakly nonlinear asymptotic expansion is valid for forcing amplitudes $\epsilon_{max} < r_G^{-0.5}$. For forcing amplitudes greater than ϵ_{max}, the asymptotic expansion diverges. To obtain an expression for the gain that is uniformly valid, we use the concept of Borel summation of an asymptotic series [11], a technique based on a generalized definition of summability. The Borel transform of the geometric series (18) is given by

$$\mathcal{B}G(t) = \sum_{n=0}^{\infty}\frac{(-r_G t^2)^n}{n!} = 1 - r_G t^2 + \frac{r_G^2 t^4}{2!} - \frac{r_G^3 t^6}{3!} + \cdots = \exp(-r_G t^2), \tag{20}$$

which is now valid for all parameters t. We then form the expression

$$B(\epsilon) = \frac{1}{\epsilon}\int_0^{\infty} e^{-t/\epsilon}\mathcal{B}G(t)dt \tag{21}$$

which, after a power expansion for small ϵ and a term-by-term integration of the resulting expressions, reproduces

$$B(\epsilon) = \sum_{n=0}^{\infty} a_n\epsilon^n. \tag{22}$$

The above procedure then suggests that $B(\epsilon)$ is asymptotic to the diverging series for small values of ϵ. We thus continue to apply Borel summation to our geometric series which results in

$$\int_0^\infty e^{-t}\mathcal{B}G(t\epsilon)dt = \int_0^\infty e^{-t}e^{-r_G\epsilon^2t^2}dt,$$
$$= \frac{\sqrt{\pi}}{2\sqrt{r_G}\epsilon}\exp\left(\frac{1}{4r_G\epsilon^2}\right)\mathrm{erfc}\left(\frac{1}{2\sqrt{r_G}\epsilon}\right). \quad (23)$$

Using this expression, we display the approximation to the weakly nonlinear gain in figure 8 and compare the asymptotic weakly nonlinear results with a self-consistent model [9] that has been found to correctly capture the fully nonlinear behavior. The details of the self-consistent model can be found in the Appendix.

We find that the Borel sum provides a reasonable approximation to the nonlinear behavior up to one order of magnitude beyond the radius of convergence of the asymptotic expansion (19). For larger forcing amplitudes, the Borel sum consistently overpredicts the gain because it scales as $1/\epsilon$. The self-consistent model saturates at a faster rate but does not show a tendency for the $m = 0$ mode to dominate over the $m = 1$ mode. These results have been obtained for each mode evolving independently and for a fixed forcing structure – an impulse near the jet exit. In figure 9, we plot the nonlinear behavior of the gain in response to the linear optimal forcing structure for each mode at $St = 0.45$. This represents the "worst-case scenario". We find that even the optimal forcing does not show a tendency for the $m = 0$ mode to dominate over the $m = 1$ mode if forced equally and independently. If both modes are forced simultaneously and with equal amplitude, we find, using the self-consistent model, that the $m = 0$ mode is even more strongly saturated than the $m = 1$ mode. This is because the nonlinear base-flow modification caused by the Reynolds stress terms of $m = 1$ forcing is significantly greater than that caused by $m = 0$ forcing. We conclude that, in response to forcing of equal amplitudes, the $m = 1$ mode will dominate over the $m = 0$ mode.

The asymptotic analysis that we have presented is based on the assumption that the ratios between the weakly nonlinear coefficients are equal. The results in figures 8 and 9 show that this is a reasonable first approximation to make. However, the overprediction in the gain curves for larger forcing amplitudes suggests that the ratios between higher-order coefficients must decrease. We would expect this from a physical point of view as well. We can model this feature by multiplying the ratio r_G by a factor $\mu < 1$ in (18). The

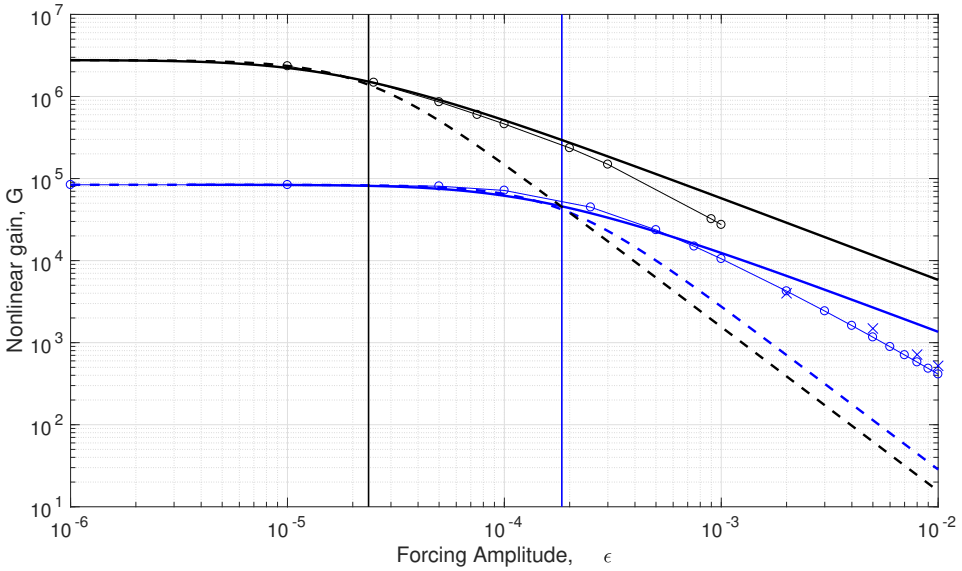

FIG. 8. The variation of the gain with forcing amplitude for fixed Gaussian forcing with $m = 0$ (blue) and $m = 1$ (black) for $St = 0.40$ at $Re = 1000$. The solid lines represent the results of the Borel summation (23), and the dashed lines represent the weakly nonlinear asymptotic expansion (19). The circles represent a self-consistent model that correctly predicts the nonlinear behavior, represented as crosses. The two vertical lines indicate, for the respective azimuthal wavenumber, the critical forcing amplitudes given by the radius of convergence of the geometric series (18).

corresponding gain curves would exhibit strong saturation even for minute reductions from unity in the value of μ. The effect of nonlinearities on the frequency response curve for $m = 0$ and $m = 1$ is displayed in figure 10. We observe a tendency for the response to become more broadband as the forcing amplitude is increased.

V. CONCLUSIONS

We have studied the effect of nonlinearities on the global frequency response of a uniform-density jet. A weakly nonlinear expansion has been employed to calculate the higher-order corrections to the linear frequency response for axisymmetric and non-axisymmetric body forcing. In particular, we focus our attention on the axisymmetric ($m = 0$) and asymmetric ($m = 1$) azimuthal modes about frequencies that are optimally excited in experiments, that

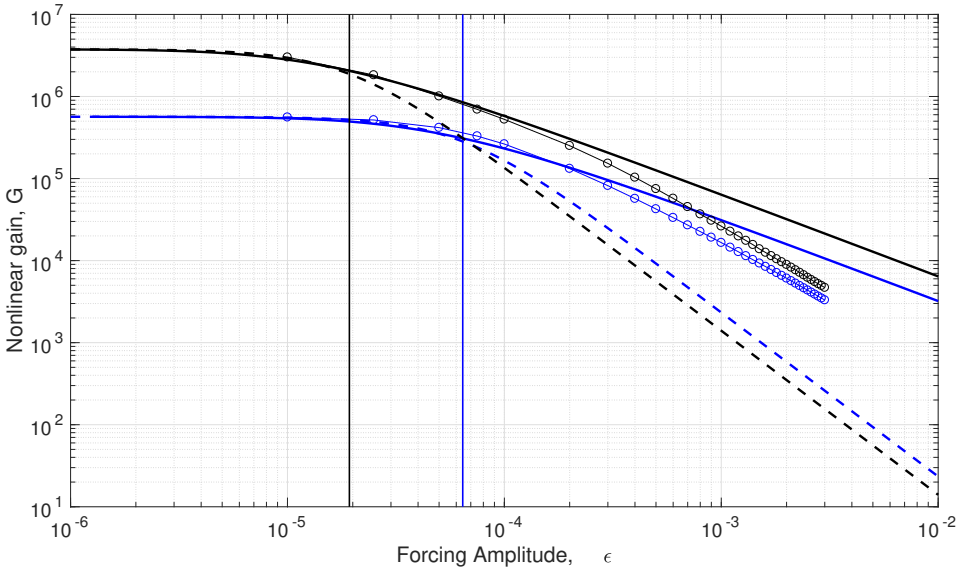

FIG. 9. The variation of the gain with forcing amplitude for the optimal linear forcing with $m = 0$ (blue) and $m = 1$ (black) for $St = 0.45$ at $Re = 1000$. The solid lines represent the results of the Borel summation (23), and the dashed lines represent the weakly nonlinear asymptotic expansion (19). The circles represent a self-consistent model that correctly predicts the nonlinear behavior. The two vertical lines indicate, for the respective azimuthal wavenumber, the critical forcing amplitudes given by the radius of convergence of the geometric series (18).

is, for Strouhal numbers around $St \sim 0.3$. We find that the expansion coefficients of the weakly nonlinear expansion describe a divergent series. While recognizing the limit in forcing amplitude beyond which the asymptotic expansion is not valid, we have derived an integral expression for the sum of the divergent series beyond this limit using a Borel summation. We find that this expression gives a pleasing approximation to the full nonlinear gain up to one order of magnitude beyond the limit of validity of the weakly nonlinear expansion. We have also compared our results with a self-consistent model that takes into account the base flow modification induced by the Reynolds stress terms of the forcing.

For infinitesimally small forcing amplitudes, the asymmetric mode of the forcing is more strongly amplified than the axisymmetric mode. However, as the forcing amplitude is increased, nonlinearity acts to saturate the flow response. Although the asymmetric mode experiences strong saturation, we do not observe a tendency for the axisymmetric mode to dominate. These results have been obtained for each mode being forced equally. In a

	$m = 0$	$m = 1$
G_1	8.40×10^4	2.78×10^6
$G_{2,2}$	5.80×10^{10}	6.45×10^{13}
$G_{1,13}$	-2.48×10^{12}	-4.97×10^{15}
$G_{1,15}$	7.85×10^{19}	2.13×10^{24}
$G_{13,13}$	3.79×10^{19}	1.02×10^{25}
$G_{2,24}$	-4.23×10^{18}	-1.84×10^{23}
$G_{3,3}$	8.06×10^{16}	2.80×10^{21}

TABLE I. Weakly nonlinear gain coefficients for $m = 0$ and $m = 1$ at $Re = 1000$ for the fixed forcing with $St = 0.40$.

real experiment, the forcing will be stochastic and distributed over all azimuthal modes. The nonlinear behaviour of each mode will be determined by the projection of the forcing onto the optimal forcing structure of each azimuthal mode. The experimental dominance of axisymmetric structures could then be explained by the axisymmetric component of the forcing having a larger amplitude than the asymmetric component of the forcing. This would correspond to a horizontal shift of the gain curves in figure 9 with respect to each other.

The presented formalism can easily be applied to configurations where the linear frequency response is used to understand other aspects of jet dynamics, for example, the production of noise in high-speed jet flows, [12]. In this case, our asymptotic approach could provide a quick estimate of nonlinear effects with minimal computational effort. In closing, we would like to point out that the asymptotic approach is expected to give better results for flows that exhibit less non-normality – e.g., strongly non-parallel flows at moderate Reynolds numbers, and for flows that exhibit supercritical bifurcations, as observed in, for example, convection.

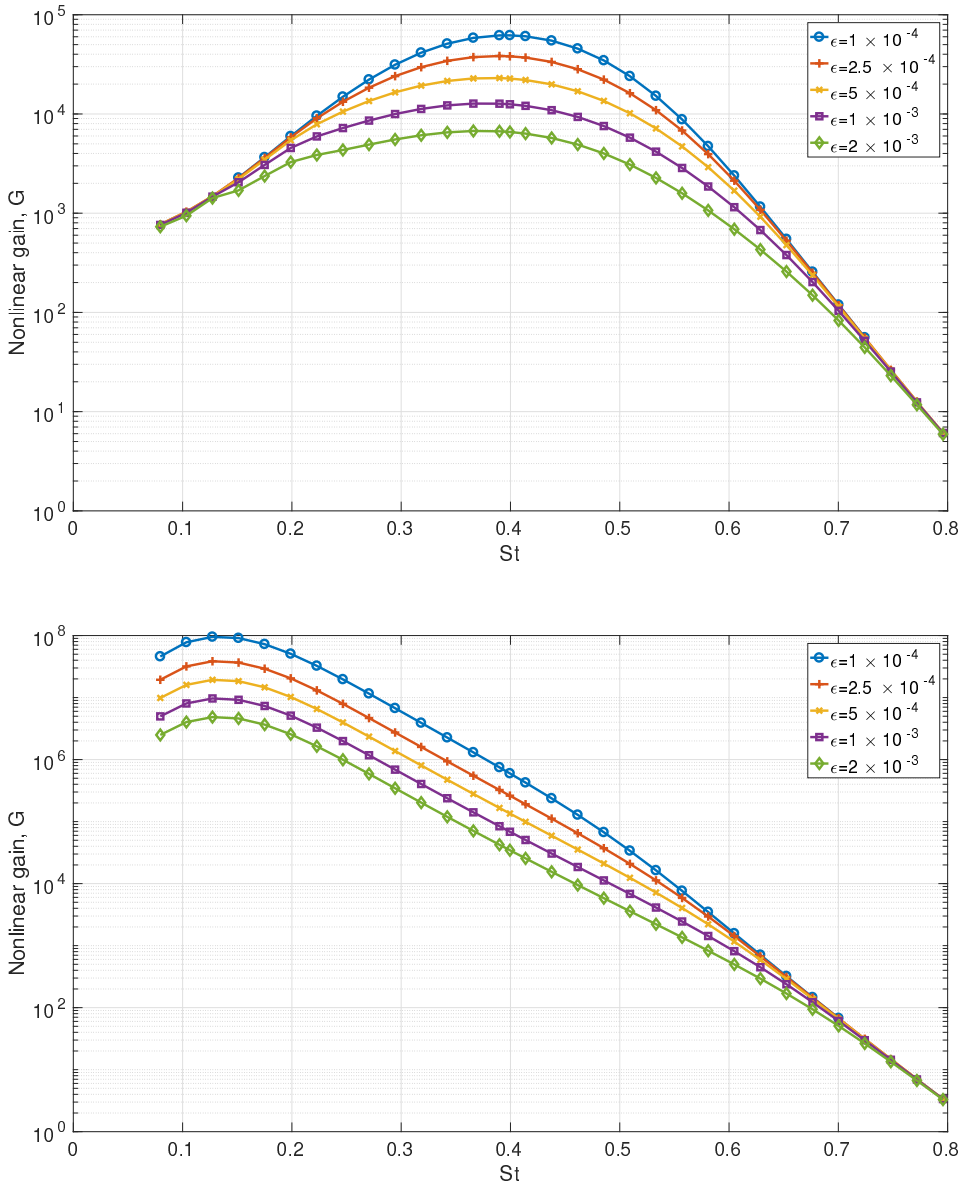

FIG. 10. Variation of the frequency response curve with forcing amplitude for fixed forcing with (a) $m = 0$ (top), and (b) $m = 1$ (bottom), at $Re = 1000$.

ACKNOWLEDGMENTS

The authors acknowledge the support of the Engineering and Physical Sciences Research Council, UK, through grant EP/I037946/1.

Appendix A: Self-consistent model

For flows far from the primary bifurcation, previous studies in a variety of flow configurations have shown that linear stability analyses around time-averaged (mean) flow profiles provide accurate predictions of the dominant nonlinear frequency content of the unsteady flow [13, 14]. Similarly, linear responses to harmonic forcing around the mean flow also provide accurate predictions of the nonlinear amplification of finite-amplitude forcing [8, 9]. In both these cases, most of the energy in the nonlinear flow is contained within the fundamental frequency, or first harmonic. Mantic-Lugo & Gallaire [9] noted this and proposed a self-consistent model that couples the nonlinear mean-flow equations with the linear perturbation equations using the Reynolds stresses. Taking into account non-axisymmetric forcing structures, this model has the form

$$\mathcal{N}(\bar{\mathbf{u}}) = -2\sum_{m=0}^{\infty} \mathrm{Re}\left(\hat{\mathbf{u}}^{*}_{m,1,1}.\nabla\hat{\mathbf{u}}_{m,1,1}\right), \tag{A1}$$

$$\sum_{m=0}^{\infty}(\mathrm{i}\omega_f\mathbf{B}-\mathbf{L}_m)\hat{\mathbf{q}}_{m,1,1} = \sum_{m=0}^{\infty}\hat{\mathbf{f}}_m e^{\mathrm{i}m\theta}, \tag{A2}$$

where $\bar{\mathbf{u}}$ is the axisymmetric mean flow, m is the azimuthal wavenumber of perturbations, and the operator $\mathbf{L}_m$ is the linearized Navier-Stokes operator for perturbations with azimuthal wavenumber m around the mean flow $\bar{\mathbf{u}}$. Different azimuthal modes are coupled through the base flow modifications caused by the Reynolds stresses. In the general case, one would have to consider the linear response to forcing at each azimuthal wavenumber. In this study, however, we focus only on forcing with azimuthal wavenumbers $m = 0$ and $m = 1$.

We solve the coupled system using the amplitude stepping algorithm proposed by Mantic-Lugo & Gallaire [9]. Starting from a small amplitude $\epsilon = 10^{-5}$, we gradually increase the amplitude. At each step, we calulcate the coupled linear response and mean flow in an iterative manner until the l^2-norm of the changes in the mean flow are less than 10^{-4}. We find that this leads to results that are sufficiently well-converged up to a certain forcing amplitude. Beyond this amplitude, we have great difficulty in obtaining converged solutions.

To verify the validity of the self-consistent model and the solution algorithm, we compare the results obtained for purely axisymmetric Gaussian forcing with results from a nonlinear direct numerical simulation (DNS) of the axisymmetric Navier-Stokes equations. For the

	$\Delta t = 0.008$	$\Delta t = 0.0125$	$\Delta t = 0.025$	$\Delta t = 0.03$
Nonlinear gain	3999	3885	3420	3135

TABLE II. Nonlinear gain for fixed Gaussian forcing with $m = 0$ and amplitude $\epsilon = 2 \times 10^{-3}$ for $St = 0.45$ at $Re = 1000$.

DNS, we use the same discretization in FreeFem++ as used for the weakly nonlinear analysis together with a characteristics-based solution algorithm with implicit time-stepping. In table II, we evaluate the effect of time-step on the nonlinear gain given by (12) for a forcing amplitude $\epsilon = 2 \times 10^{-3}$. We choose $\Delta t = 0.008$ to compare the gain with the self-consistent model for a range of forcing amplitudes. This comparison is shown in figure 8. We find that the self-consistent model provides a reasonable estimate of the nonlinear gain, but under-predicts the gain at higher forcing amplitudes. We attribute this to the effect of higher-order harmonics, which are not captured in the self-consistent model. Nevertheless, the results show that the self-consistent model provides a useful and accurate estimate for the fully nonlinear behaviour.

[1] S. C. Crow and F. H. Champagne, "Orderly structure in jet turbulence," *J. Fluid Mech.*, vol. 48, p. 547, 1971.

[2] A. Michalke, "Survey on jet instability theory," *Prog. Aerosp. Sci.*, vol. 21, pp. 159–199, 1984.

[3] J. I. Jimenez-Gonzalez, P. Brancher, and C. Martinez-Bazan, "Modal and non-modal evolution of perturbations for parallel round jets," *Phys. Fluids*, vol. 27, p. 044105, 2015.

[4] X. Garnaud, L. Lesshafft, P. Schmid, and P. Huerre, "Modal and transient dynamics of jet flows," *Phys. Fluids*, vol. 25, no. 044103, 2013.

[5] D. Sipp and O. Marquet, "Characterization of noise amplifiers with global singular modes: the case of the leading-edge flat plate boundary layer," *Theor. Comp. Fluid Dyn.*, vol. 27, pp. 617–635, 2013.

[6] J.-M. Chomaz, "Global instabilities in spatially developing flows: Non-normality and nonlinearity," *Ann. Rev. Fluid Mech.*, vol. 37, pp. 357–392, 2005.

[7] P. Schmid, "Nonmodal stability theory," *Ann. Rev. Fluid Mech.*, vol. 39, pp. 129–162, 2007.

[8] X. Garnaud, L. Lesshafft, P. Schmid, and P. Huerre, "The preferred mode of incompressible jets: linear frequency response analysis," *J. Fluid Mech.*, vol. 716, pp. 189–202, 2013.

[9] V. Mantic-Lugo and F. Gallaire, "Self-consistent model for the saturation mechanism of the response to harmonic forcing in the backward-facing step flow," *J. Fluid Mech.*, vol. 794, pp. 777–797, 2016.

[10] S. C. Reddy, P. J. Schmid, and D. S. Henningson, "Pseudospectra of the orr-sommerfeld operator," *SIAM Journal on Applied Mathematics*, vol. 53, no. 1, pp. 15–47, 1993.

[11] C. M. Bender and S. A. Orszag, *Advanced mathematical methods for scientists and engineers I.* Springer Science & Business Media, 1999.

[12] J. Jeun, J. W. Nichols, and M. R. Jovanović, "Input-output analysis of high-speed axisymmetric isothermal jet noise," *Physics of Fluids (1994-present)*, vol. 28, no. 4, p. 047101, 2016.

[13] D. Barkley, "Linear analysis of the cylinder wake mean flow." *Europhys. Lett.*, vol. 75, pp. 750–756, 2006.

[14] D. Sipp and A. Lebedev, "Global stability of base and mean flows: a general approach and its applications to cylinder and open cavity flows." *J. Fluid Mech.*, vol. 593, pp. 333–358, 2007.